A simple bilayered magnetoelectric random access memory cell based on electric-field controllable domain structure

Jia-Mian Hu, Zheng Li, Jing Wang, Jing Ma, Y. H. Lin, and C. W. Nan[a)]
Department of Materials Science and Engineering and State Key Laboratory of New Ceramics and Fine Processing, Tsinghua University, Beijing 100084, China

(Received 28 May 2010; accepted 15 June 2010; published online 18 August 2010)

By considering the domain wall scattering in ferromagnetic striped-domain structure, we present a simple bilayered magnetoelectric random access memory cell with a ferromagnetic thin film grown on a ferroelectric layer. The calculations show that the striped-domain structure in the ferromagnetic film can change into a single-domain structure upon applying an electric field to the ferroelectric layer. As a result, the presence (absence) of the domain walls in response to the striped-domain (single-domain) state can cause an abrupt change in the film resistivity, which could be employed for memory applications accordingly. © *2010 American Institute of Physics*.
[doi:10.1063/1.3463408]

An electric-field-controlled magnetic memory device—namely, the magnetoelectric random access memory (MERAM), which combines the best aspects of ferroelectric (FE) random access memory and magnetic random access memory devices in terms of electric-field-writing and nondestructive readout, has recently provoked intensive scientific and technological interests in the fields of spintronics and multiferroics.[1–6] Such MERAM devices could be constructed with a spin-valve[7] or magnetic tunnel junction (MTJ) (Ref. 8) element attached to a FE-antiferromagnetic $BiFeO_3$,[2,3] a magnetoelectric (ME) antiferromagnetic Cr_2O_3,[4] or a FE layer.[5,6] In these multilayer heterostructures, bistable resistance states could result from the different magnetic configurations (e.g., parallel or antiparallel) in the spin-valve (via giant magnetoresistance effect[9]) or MTJ unit (via tunneling magnetoresistance effect[8]), based on ME coupling[10–13] between the free magnetic layer of the spin-valve or MTJ and its attached FE layer.

In this work, we present a novel MERAM device simply consisting of a ferromagnetic (FM) thin film grown on a FE layer, without the magnetic trilayers required in the spin-valve or MTJ-based MERAMs. As shown below, the in-plane 180° periodic domain structure in the FM film can be effectively modulated by an electric field applied to the FE layer, or even changes into a single-domain structure at a certain critical electric field. Furthermore, by considering the domain wall scattering in such FM striped-domain structure,[14,15] a sharp resistivity change could happen due to the presence and absence of the walls, which could be exploited in memory devices accordingly. The presented concept of the simple bilayered MERAM device might offer new trends toward novel multiferroic devices through domain wall engineering.

Consider a FM/FE bilayered heterostructure wherein the FM layer shows in-plane periodic 180° domains, i.e., the domains orient along the same axis in the film plane but with opposite polarity, along with separating 180° Néel wall, as schematically shown in Fig. 1(a). Such striped magnetic domain structure could be obtained through control of the sample geometry as well as proper treatment processing.[16–18,22] A transverse electric field E is then applied to the bottom FE layer to modulate the domain structure of the FM film. Figure 1(b) shows a close-up view of the 180° Néel wall in the FM layer. As seen, the spins in the wall rotate gradually in the film plane, with no free poles shown at the sample surface. The length (L), width (W), and thick-

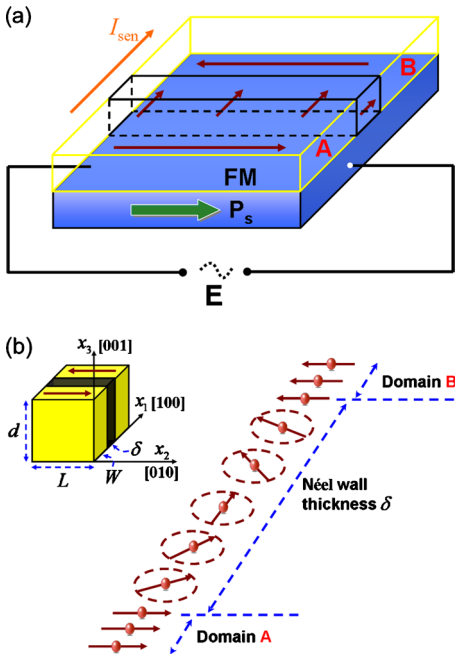

FIG. 1. (Color online) (a) Schematic of a bilayered MERAM cell, consisting of a thin FM film with in-plane periodic 180° domains (i.e., domains A and B and the Néel wall between them) grown on a FE layer. A transverse electric field E is applied to the FE layer with a spontaneous polarization P_s to modulate the magnetic domain structure. The sensing current I_{sen} is applied perpendicular to the Néel wall to detect the resistance change in the FM film. (b) Structure of the 180° Néel wall in the FM film. The length (L), width (W), and thickness (d) directions of its adjacent domains are set to be along the three principle crystal axes, i.e., the [010], [100], and [001], respectively. δ is the domain wall thickness.

[a)]Electronic mail: cwnan@tsinghua.edu.cn.

ness (d) directions of the domains are considered to be along the three principal crystal axes, respectively.

The total free energy F_{tot} of a domain period, i.e., a single striped domain (e.g., domain A) with a 180° Néel wall, can be expressed as,[16]

$$F_{tot} = F_d + F_w, \tag{1}$$

where F_d and F_w denote the free energy contributions of the magnetic domain and domain wall, respectively. Among them,

$$F_w = \sigma_w \frac{d}{W}, \tag{2}$$

where σ_w is the energy density of the domain wall.[17] Equation (2) simply indicates that F_w depends linearly on the wall size (proportional to sample thickness d) and the number of walls (inversely proportional to the domain size). It has been demonstrated previously that an in-plane magnetization switching can be induced by applying an electric field on the FM/FE layered heterostructure.[6,12] Based on the principle of such an in-plane magnetization switching, the magnetic domain structure can be effectively modulated by the external electric field. For illustration, our calculations are performed for FM Fe–Co alloys, including the hexagonal (0001)-oriented $Co_{0.9}Fe_{0.1}$ and the cubic (001)-oriented $Fe_{0.7}Co_{0.3}$, which are often used as the free layers of the MTJ due to their magnetically soft nature.[19] The FE layer is chosen to be $Pb(Zn_{1/3}Nb_{2/3})O_3$–$PbTiO_3$ (PZN–PT) with high piezoelectric response ($d_{33} \sim 2500$ pm/V and $d_{31} \sim -1100$ pm/V).[20]

Let us consider that the spins in the domains and the walls rotate by a certain angle φ under the applied electric field, as shown in Fig. 2(a). The initial magnetization directions in the magnetic domains A and B are assumed to be parallel and antiparallel to the crystal axis x_2, i.e., along the [010] and [0$\bar{1}$0] directions, respectively. Then the total free energy change during the rotation process can be written as,

$$\Delta F_{tot} = \Delta F_d + \Delta F_w. \tag{3}$$

If $\Delta F_{tot} < 0$, the new magnetization direction becomes more energetically favorable, i.e., the in-plane spin rotation can happen. Specifically, the in-plane free energy density change in the magnetic domain, i.e., ΔF_d, can be derived as,[6,12]

$$\Delta F_d = \left[\frac{1}{2}\mu_0 M_S^2 \frac{C(k)d}{W} + B_1(\varepsilon_{22} - \varepsilon_{11})\right] \sin^2 \varphi, \tag{4a}$$

for a hexagonal (0001)-oriented $Co_{0.9}Fe_{0.1}$ film with uniaxial anisotropy, and,

$$\Delta F_d = \left[K_1 + \frac{1}{2}\mu_0 M_S^2 \frac{C(k)d}{W} + B_1(\varepsilon_{22} - \varepsilon_{11})\right] \sin^2 \varphi - K_1 \sin^4 \varphi, \tag{4b}$$

for a cubic (001)-oriented $Fe_{0.7}Co_{0.3}$ film with in-plane biaxial anisotropy. Here K_1 and B_1 denote the magnetocrystalline coefficient and magnetoelastic constant, respectively; μ_0 and M_s are the vacuum permeability and the saturation magnetization of the FM layer, respectively; W and d are, respectively, the width and thickness of the magnetic domains [Fig. 1(b)]; $C(k)$ is a coefficient depending on the aspect ratio k

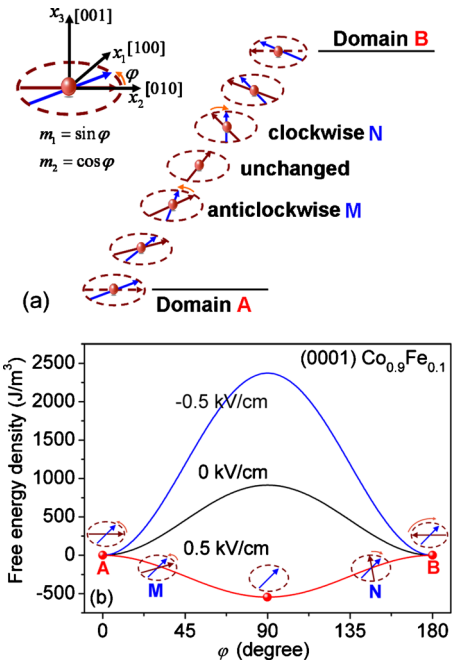

FIG. 2. (Color online) (a) Schematic diagram of the electric-field-induced spin rotation in a thin FM film with in-plane striped-domain structure. The spins in both the two adjacent magnetic domains (i.e., A and B) and the Néel wall tend to rotate away from their initial magnetization directions under external electric fields. (b) Free energy density change in (0001)-oriented $Co_{0.9}Fe_{0.1}$ film as a function of the rotation angle φ with electric fields varying from −0.5 to 0.5 kV/cm. The arrows within ellipses describe the trends of spin rotation. As seen, the spins in both the domains and the Néel wall rotate to the crystal axis x_1 anticlockwise (e.g., A and M) or clockwise (e.g., B and N) under an electric field of about 0.5 kV/cm, leading to an overall uniform magnetization and thus a single-domain structure.

$= L/W$. ε_{11} and ε_{22} are the elastic strains along the two in-plane crystal axes x_1 and x_2, which can be expressed as,

$$\varepsilon_{11} = \varepsilon_0 + p d_{31} E,$$

$$\varepsilon_{22} = \varepsilon_0 + p d_{33} E, \tag{5}$$

under a transverse electric field E. Here d_{33} and d_{31} are piezoelectric coefficients of the FE layer, and ε_0 is the residual strain. The interfacial coupling factor p with $0 \le p \le 1$ is introduced to characterize the possible loss of elastic coupling interaction due to imperfect interface contact. Thus, Eqs. (4a) and (4b) can be further written as,

$$\Delta F_d = K_u \sin^2 \varphi,$$

$$K_u = \frac{1}{2}\mu_0 M_S^2 \frac{C(k)d}{W} + B_1 p(d_{33} - d_{31})E, \tag{6a}$$

for the (0001)-oriented $Co_{0.9}Fe_{0.1}$ film, and,

$$\Delta F_d = K_A \sin^2 \varphi + K_B \sin^4 \varphi,$$

$$K_A = K_1 + \frac{1}{2}\mu_0 M_S^2 \frac{C(k)d}{W} + B_1 p(d_{33} - d_{31})E, \quad K_B = -K_1, \tag{6b}$$

for the (001)-oriented $Fe_{0.7}Co_{0.3}$ film.

Moreover, the energy density of the domain wall, i.e., σ_w, can be given by the sum of the exchange and anisotropy energy densities, i.e.,

$$\sigma_w = \sigma_{ex} + \sigma_a. \tag{7}$$

Here the exchange energy contribution σ_{ex} can be deduced as,[21]

$$\sigma_{ex} = A\left(\frac{d\varphi}{dx_3}\right)^2, \tag{8}$$

for a 180° Néel wall lying in the x_1x_2 plane, where A is the exchange constant. The anisotropy energy contribution σ_a bears the same expressions as those in the domains [see Eqs. (6a) and (6b)], since we consider the energy density change during the switching process herein. Furthermore, the total wall energy density σ_w can be obtained by integrating these energy contributions over the thickness of the wall, i.e.,

$$\sigma_w = \int_{-\infty}^{\infty}\left[A\left(\frac{d\varphi}{dx_3}\right)^2 + K_u \sin^2\varphi\right]dx = 4\sqrt{AK_u}, \tag{9a}$$

for the (0001)-oriented $Co_{0.9}Fe_{0.1}$ film, and,

$$\sigma_w = \int_{-\infty}^{\infty}\left[A\left(\frac{d\varphi}{dx_3}\right)^2 + K_A \sin^2\varphi + K_B \sin^4\varphi\right]dx = 2\sqrt{A}\frac{\sqrt{K_A}K_B + (K_A+K_B)\sqrt{-K_B}\,\mathrm{atanh}\left(\frac{K_B}{\sqrt{-K_AK_B}}\right)}{K_B}, \tag{9b}$$

for the (001)-oriented $Fe_{0.7}Co_{0.3}$ film. Following Kittel's scaling law,[16,17] the equilibrium domain width W is considered to be proportional to the film thickness d and wall energy density σ_w, i.e.,

$$W \propto \sqrt{\sigma_w d}. \tag{10}$$

By comparing this with Eq. (2), it can be seen that the change in the domain wall energy, i.e., ΔF_w, shows no dependence on the direction cosine m_1 or rotation angle φ, thereby not contributing to the total free energy change ΔF_{tot} [Eq. (3)].[6,12]

On the other hand, the domain wall thickness δ in such in-plane FM striped-domain structure can be approximated by the formula,

$$\delta = \pi\sqrt{\frac{A}{K_u}}, \tag{11a}$$

for the hexagonal $Co_{0.9}Fe_{0.1}$ with uniaxial magnetic anisotropy,[21] and,

$$\delta = 2\sqrt{2}\sqrt{\frac{A}{K_A}}, \tag{11b}$$

for the cubic $Fe_{0.7}Co_{0.3}$ with biaxial magnetic anisotropy,[17] with the coefficients K_u and K_A given in Eqs. (6a) and (6b), respectively. From Eqs. (9a), (9b), (10), (11a), and (11b), it can be seen that both the domain width W and the wall thickness δ can be effectively modulated by the electric field applied to the FE layer.

We now discuss the domain structure changes under the external electric field. The electric-field-induced magnetization switching features of the domain period can be described through minimization of ΔF_{tot} with respect to m_1 or φ, by using usual materials parameters.[22] For example, Fig. 2(b) shows the total free energy profile changes in the hexagonal (0001) $Co_{0.9}Fe_{0.1}$ under different electric fields applied to the bottom FE layer, with the interfacial coupling factor p set to be 1 (i.e., a perfect interface which allows the full transfer of the elastic strains). As seen, the free energy minimum appears at $\varphi=0°$ or 180° ($m_1=0$) at $E=0$ and -0.5 kV/cm [see the solid dots in Fig. 2(b)] and the total free energy change ΔF_{tot} remains positive, indicating that the stable magnetization orientations are kept parallel and antiparallel to the crystal axis x_2 for the domains A and B, i.e., along the [010] and [0$\bar{1}$0] directions, respectively. However, a positive electric field E [parallel to the polarization direction P_s of the FE layer, see Fig. 1(a)] of 0.5 kV/cm can shift the energy minimum to the angle $\varphi=90°$ ($m_1=1$). In this case, the spins in both the magnetic domains and the Néel wall would align parallel to the crystal axis x_1, i.e., the [100] direction, which further leads to the formation of a single-domain structure.

Figures 3(a) and 3(b) further show the electric-field dependence of the wall energy density σ_w and the wall thickness δ in the (0001)-oriented $Co_{0.9}Fe_{0.1}$ film under different interfacial coupling factors, respectively. As seen, the wall energy density σ_w gradually decreases to zero at a certain critical electric field E^{cr}, which is inversely proportional to the interfacial coupling factor p, i.e.,

$$E^{cr} = -\frac{\mu_0 M_S^2 C(k) d}{2WpB_1(d_{31}-d_{33})}. \tag{12}$$

$E^{cr}=0.313$ kV/cm as $p=1$, as shown in Fig. 3(a). In consequence, the domain width W also reduces when E^{cr} is approached [see Eq. (10)]. As the electric field surpasses E^{cr}, the domain width W vanishes to zero accordingly corresponding to the annihilation of the initial striped domains [see the insets of Fig. 3(a)], and a single-domain structure with the magnetization switching by 90° from the initial states appears. In comparison, the domain wall gradually expands at the expense of its neighboring striped domains with increasing electric field. It should be noted that the wall thickness δ increases very sharply in the immediate vicinity of E^{cr}, which is in relation to the presence of a single-domain structure, as shown in Fig. 3(b).

For clear illustration, Fig. 3(c) intuitively shows such a transition from striped-domain to single-domain in the (0001)-oriented $Co_{0.9}Fe_{0.1}$ film. As shown, the initial magnetizations in the striped domains are along the crystal axis x_2, i.e., the [010] and [0$\bar{1}$0] directions. However, the magnetization vectors rotate by 90° to the crystal axis x_1 abruptly at the critical electric field E^{cr} [see the insets of Fig. 3(c)], which further leads to the formation of a single-domain structure. Nevertheless, this single-domain structure in the (0001) $Co_{0.9}Fe_{0.1}$ film is not stable and would turn back into its initial striped-domain state when switching off the electric field.

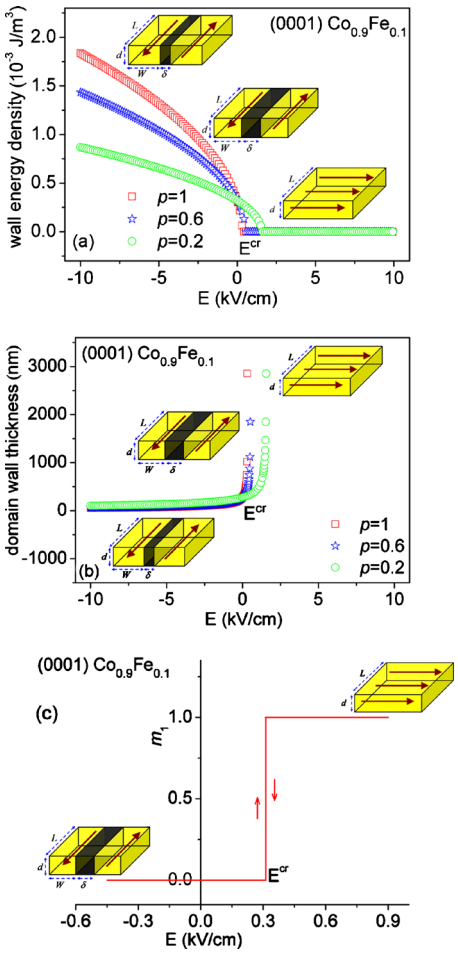

FIG. 3. (Color online) Electric-field dependences of (a) the domain wall energy and (b) the wall thickness in the (0001)-oriented $Co_{0.9}Fe_{0.1}$ film with different interfacial coupling factors p. (c) Electric-field-induced transition between striped-domain and single-domain structure in the (0001)-oriented $Co_{0.9}Fe_{0.1}$ film associated with the in-plane 90° magnetization switching from the crystal axis $x_2(m_1=0)$ to $x_1(m_1=1)$ in the domains. The insets are the profiles of the (0001)-oriented $Co_{0.9}Fe_{0.1}$ film, which schematically shows the evolution process of the magnetic domain structures with varying electric fields.

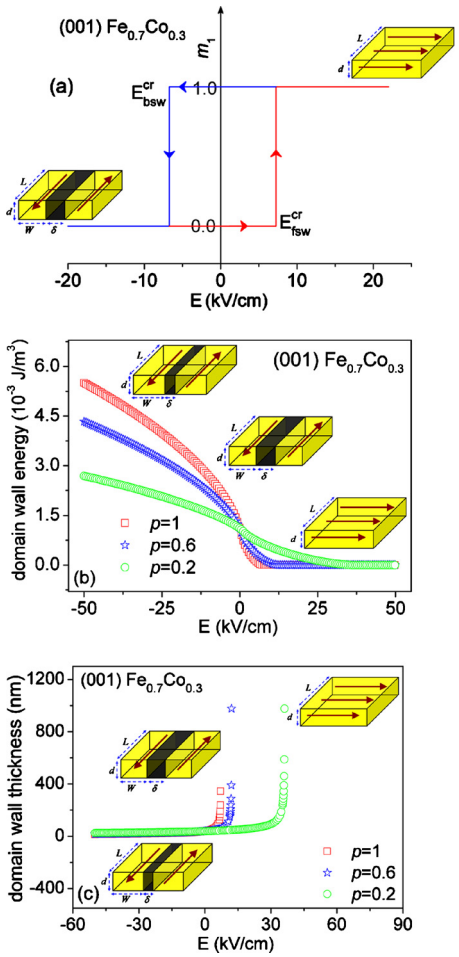

FIG. 4. (Color online) (a) Electric-field-induced transition between striped-domain and single-domain structure in the (001)-oriented $Fe_{0.7}Co_{0.3}$ film associated with the in-plane 90° magnetization switching from the crystal axis $x_2(m_1=0)$ to $x_1(m_1=1)$ in the domains. A hysteresis loop of the direction cosine m_1 dependent on the applied electric field is observed. Electric-field dependences of (b) the domain wall energy and (c) the wall thickness in the (001)-oriented $Fe_{0.7}Co_{0.3}$ film with different interfacial coupling factors p. The insets are the profiles of the (001)-oriented $Fe_{0.7}Co_{0.3}$ film, which schematically shows the evolution process of the domain structures with varying electric fields.

In comparison with the hexagonal (0001)-oriented $Co_{0.9}Fe_{0.1}$ film, the cubic (001)-oriented $Fe_{0.7}Co_{0.3}$ film presents a different behavior of the electric-field-induced transition between multidomain and single-domain structure, as shown in Fig. 4(a). As seen, the FM film changes from its initial striped-domain state to a single-domain state at a critical forward switching electric field E_{fsw}^{cr} of about 7.25 kV/cm. This single-domain state can be retained even after the external electric field is removed but then resumed back to the striped-domain state at a critical back switching electric field E_{bsw}^{cr} of about −6.74 kV/cm. Such a hysteresis domain structure change can be attributed to the positive magnetocrystalline constant K_1 of the (001)-oriented $Fe_{0.7}Co_{0.3}$ film, as reported in the previous work.[6] The corresponding forward and back switching electric field during this process, i.e., E_{fsw}^{cr} and E_{bsw}^{cr}, respectively, can be expressed as,

$$E_{fsw}^{cr} = -\frac{2K_1 + \mu_0 M_s^2 \frac{C(k)d}{W}}{2B_1(d_{33} - d_{31})}, \tag{13a}$$

$$E_{bsw}^{cr} = -\frac{2K_1 - \mu_0 M_s^2 \frac{C(k)d}{W}}{2B_1(d_{31} - d_{33})}. \tag{13b}$$

The electric-field dependences of the domain wall energy σ_w and the wall thickness δ in the (001)-oriented $Fe_{0.7}Co_{0.3}$ film are shown in Figs. 4(b) and 4(c), respectively, which are closely analogous to those in the hexagonal (0001)-oriented $Co_{0.9}Fe_{0.1}$ film [Figs. 3(a) and 3(b)], indicating a similar evolution process of the domain structure.

Now let us discuss how this electric-field-induced transition between multidomain and single-domain structure is related to a high and low resistance state, which might offer application potential for a novel bilayered MERAM device. Normally, the ordinary magnetoresistance of pure magnetic materials contains two major parts.[14] The first part comes from the so-called anisotropic magnetoresistance (AMR) effect,[24] which relates the orientation of the magnetization to the sensing current I_{sen} in the ferromagnet as,

$$\rho_{AMR} = \rho_{\perp} + (\rho_{\parallel} - \rho_{\perp})\cos^2\theta, \tag{14}$$

where ρ_{AMR} is the resistivity from the AMR effect, θ is the angle between the average magnetization and I_{sen}; and $\rho_{\perp}$ and $\rho_{\parallel}$ are, respectively, the resistivity for $\theta=90°$ and $\theta=0°$, which are related to the striped and single-domain states in our bilayered MERAM device, respectively, since the sensing current I_{sen} is applied perpendicular to the striped-domain structure [see Fig. 1(a)]. Hence, a change in the resistivity ρ_{AMR} would occur associated with the electric-field-induced striped-domain–single-domain transition. Such AMR effect could be modulated by an external electric field, as demonstrated in a recent experimental work,[25] where thin $Co_{0.5}Fe_{0.5}$ interdigitated electrodes were deposited on lead zirconate titanate substrate and an electric-field-induced AMR resistivity change in about 0.08% was observed in the absence of a magnetic field.[25]

The other contribution comes from the domain wall scattering, which is significantly enhanced in the striped-domain structure.[14,15] For example, a resistivity change up to 1% between the striped-domain state and the single-domain state has been observed in a thin film of cobalt,[15] which is much larger than the contribution from the AMR effect.[25] The resistivity from the domain walls in the striped-domain structure, i.e., ρ_{wall}, varies with the domain wall thickness δ as,[15]

$$\rho_{wall} \propto \frac{1}{4\delta^2}\left(\frac{h\nu_F}{E_{ex}}\right)^2, \tag{15}$$

where ν_F and E_{ex} are the Fermi velocity and the exchange energy, respectively. It can be seen from Eq. (15) that the ρ_{wall} decreases rapidly with increasing wall thickness δ and finally vanishes when the FM film is in a single-domain state [i.e., an infinite δ, see Figs. 3(b) and 4(c)].

Thus, the total resistivity ρ_{tot} of the FM film in the bilayered MERAM device can be deduced as,

$$\rho_{tot} = \begin{cases} \rho_{\perp} + \rho_{wall}, & \text{for a striped domain case} \\ \rho_{\parallel}, & \text{for a single domain case.} \end{cases} \tag{16}$$

Figures 5(a) and 5(b) schematically shows such electric-field-induced resistivity changes in the (0001)-oriented $Co_{0.9}Fe_{0.1}$ and (001)-oriented $Fe_{0.7}Co_{0.3}$ films, respectively. By neglecting the relatively small contribution from the AMR effect, the total resistivity change between the striped-domain state at $E=0$ and the single-domain state can be estimated as about 1% as in Ref. 15. These high and low resistance states can be used to determine the memory state "1" or "0," which consequently allows a nondestructive readout of the input information (e.g., positive and negative electric fields). Specifically, a hysteresis loop of the device resistance dependent on the applied electric field is obtained for the cubic (001)-oriented $Fe_{0.7}Co_{0.3}$ film, whereby a nonvolatile memory cell can be acheived.[6]

Thus, a novel electric-write electric-read MERAM device can be implemented by virtue of a simple FM/FE bilayered heterostructure, with the high and low resistance states associated with the electric-field-induced transition between striped-domain and single-domain structure in the FM film based on domain wall scattering. The main advantage of the bilayered MERAM device lies in its relative simple heterostructure, despite its relatively low ratio of resistivity change as compared to the spin-valve or MTJ-based MERAMs with spin-dependent scattering or tunneling. However, larger resistance change could be obtained by reducing the domain wall thickness [Eq. (15)], or by employing the colossal magnetoresistance effect,[26] say, replacing the ordinary FM film by perovskite manganites like $(La,Sr)MnO_3$ with competing ground states, wherein the resistivity is very sensitive to strain.[27] Thus, the presented concept of the simple bilayered MERAM device could offer interesting application potential for a nonvolatile, fast, and low power-consumed memory device through domain wall engineering, which is considered to be an important trend toward novel multiferroic devices.[28]

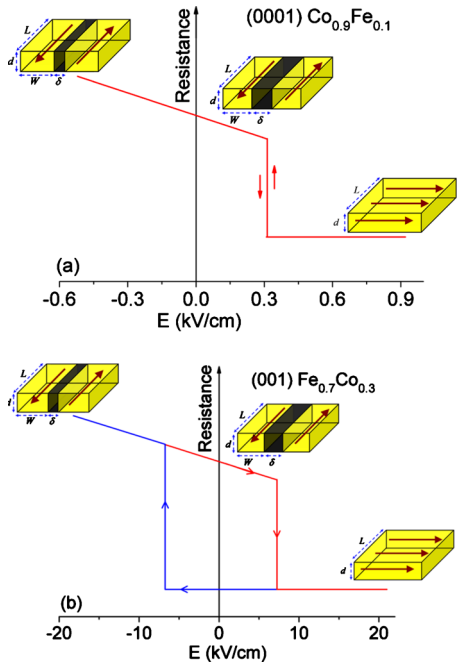

FIG. 5. (Color online) Electric-field-induced resistivity changes in (a) the (0001)-oriented $Co_{0.9}Fe_{0.1}$ and (b) the (001)-oriented $Fe_{0.7}Co_{0.3}$ films accompanied with the striped-domain–single-domain transition. A hysteresis electric-field dependence of the resistivity is observed for the (001)-oriented $Fe_{0.7}Co_{0.3}$ film. Here ρ_0 denotes the resistivity of the corresponding FM film in the single-domain state.

This work was supported by the NSF of China (Grant Nos. 50832003 and 50921061) and the National Basic Research Program of China (Grant No. 2009CB623303).

[1] W. Eerenstein, N. D. Mathur, and J. F. Scott, Nature (London) **442**, 759 (2006).
[2] H. Béa, M. Gajek, M. Bibes, and A. Barthélémy, J. Phys.: Condens. Matter **20**, 434221 (2008).
[3] M. Bibes and A. Barthélémy, Nature Mater. **7**, 425 (2008).
[4] X. Chen, A. Hochstrat, P. Borisov, and W. Kleemann, Appl. Phys. Lett. **89**, 202508 (2006).
[5] N. A. Pertsev and H. Kohlstedt, Appl. Phys. Lett. **95**, 163503 (2009).
[6] J. M. Hu, Z. Li, J. Wang, and C. W. Nan, J. Appl. Phys. **107**, 093912 (2010).
[7] B. Dieny, V. S. Speriosu, S. Metin, S. S. P. Parkin, B. A. Gurney, P. Baumgart, and D. R. Wilhoit, J. Appl. Phys. **69**, 4774 (1991).
[8] J. S. Moodera, L. R. Kinder, T. M. Wong, and R. Meservey, Phys. Rev. Lett. **74**, 3273 (1995).
[9] M. N. Baibich, J. M. Broto, A. Fert, F. Nguyen Van Dau, F. Petroff, P. Etienne, G. Creuzet, A. Friederich, and J. Chazelas, Phys. Rev. Lett. **61**,

2472 (1988).
[10]Y. H. Chu, L. W. Martin, M. B. Holcomb, M. Gajek, S. J. Han, Q. He, N. Balke, C. H. Yang, D. Lee, W. Hu, Q. Zhan, P. L. Yang, A. Fraile-Rodriguez, A. Scholl, S. X. Wang, and R. Ramesh, Nature Mater. **7**, 478 (2008).
[11]C. W. Nan, M. I. Bichurin, S. X. Dong, D. Viehland, and G. Srinivasan, J. Appl. Phys. **103**, 031101 (2008).
[12]J. M. Hu and C. W. Nan, Phys. Rev. B **80**, 224416 (2009).
[13]C.-G. Duan, S. S. Jaswal, and E. Y. Tsymbal, Phys. Rev. Lett. **97**, 047201 (2006).
[14]M. Viret, D. Vignoles, D. Cole, J. M. D. Coey, W. Allen, D. S. Daniel, and J. F. Gregg, Phys. Rev. B **53**, 8464 (1996).
[15]J. F. Gregg, W. Allen, K. Ounadjela, M. Viret, M. Hehn, S. M. Thompson, and J. M. D. Coey, Phys. Rev. Lett. **77**, 1580 (1996).
[16]C. Kittel, Phys. Rev. **70**, 965 (1946).
[17]G. Catalan, J. F. Scott, A. Schilling, and J. M. Gregg, J. Phys.: Condens. Matter **19**, 022201 (2007).
[18]P. D. Sparks, N. P. Stern, D. S. Snowden, B. A. Kappus, J. G. Checkelsky, S. S. Harberger, A. M. Fusello, and J. C. Eckert, J. Magn. Magn. Mater. **272–276**, E1339 (2004).
[19]S. Ikeda, J. Hayakawa, Y. M. Lee, F. Matsukura, Y. Ohno, T. Hanyu, and H. Ohno, IEEE Trans. Electron Devices **54**, 991 (2007).
[20]S. E. Park and T. R. Shrout, J. Appl. Phys. **82**, 1804 (1997).
[21]B. D. Cullity and C. D. Graham, *Introduction to Magnetic Materials*, 2nd ed. (Wiley, New York, 2009).
[22]The parameters (in SI units) used for numerical calculations are as follows. For hexagonal (0001)-oriented $Co_{0.9}Fe_{0.1}$, $M_s=1.59\times10^6$ A/m, $B_1=-8.1\times10^6$ J/m^3 (Refs. 10 and 23); for cubic (001)-oriented $Fe_{0.7}Co_{0.3}$, $M_s=1.91\times10^6$ A/m, $B_1=-1.43\times10^6$ J/m^3, $K_1=3.6\times10^4$ J/m^3 [Ref. 6]; the exchange constant $A=7\times10^{-12}$ J/m (Ref. 21); C(k)=0.096 as $k=2$ (Ref. 6), $W=500$ nm [the domain size is set to be constant for simplicity, which actually follows Kittel's scaling law, see Eq. (10)], $d=3$ nm. The in-plane ferromagnetic striped-domain structure can be obtained in the sample of such a geometry with proper demagnetizing processing (Ref. 16).
[23]D. Sander, Rep. Prog. Phys. **62**, 809 (1999).
[24]I. A. Campbell and A. Fert, in *Ferromagnetic Materials*, edited by E. P. Wohlfarth (North-Holland, Amsterdam, 1982), Vol. 3.
[25]H. Boukari, C. Cavaco, W. Eyckmans, L. Lagae, and G. Borghs, J. Appl. Phys. **101**, 054903 (2007).
[26]Y. Tokura, Y. Tomioka, H. Kuwahara, A. Asamitsu, Y. Moritomo, and M. Kasai, J. Appl. Phys. **79**, 5288 (1996).
[27]K. H. Ahn, T. Lookman, and A. R. Bishop, Nature (London) **428**, 401 (2004).
[28]E. K. H. Salje, ChemPhysChem **11**(5), 940 (2010).